Results in Surfaces and Interfaces 14 (2024) 100175

Contents lists available at ScienceDirect

Results in Surfaces and Interfaces

journal homepage: www.elsevier.com/locate/rsurfi

Amino acid ionic liquids as efficient catalysts for CO_2 capture: A combined static and dynamic approach

Abdul Rajjak Shaikh [a,*], Anna Vidal-López [b,c], Artur Brotons-Rufes [b], Jason J. Pajski [a,d], Sadain Zafar [a,e], Raisul Awal Mahmood [a,f], Muhammad Usman Khan [a,g], Albert Poater [b,*], Mohit Chawla [h,*], Luigi Cavallo [h,*]

[a] Department of Research and Innovation, STEMskills Research and Education Lab Private Limited, Faridabad, Haryana, 121002, India
[b] Institut de Química Computacional i Catàlisi and Departament de Química, Universitat de Girona, C/ Maria Aurèlia Capmany 69, 17003, Girona, Catalonia, Spain
[c] Department of Chemistry, Universitat Autònoma de Barcelona, Cerdanyola Del Vallès, Catalonia, 08193, Spain
[d] Department of Chemistry, East Carolina University, Greenville, NC, 27858, USA
[e] Université de Lille, CNRS, UMR 8523 – PhLAM – Laboratoire de Physique des Lasers, Atomes et Molécules, CERLA – Centre D'Etudes et de Recherche Lasers et Applications, F-59000, Lille, France
[f] Department of Chemistry, Kyungpook National University, Daegu, Republic of Korea
[g] Department of Chemistry, University of Okara, Okara, 56300, Pakistan
[h] King Abdullah University of Science and Technology (KAUST), Physical Sciences and Engineering Division, KAUST Catalysis Center, Thuwal, 23955-6900, Saudi Arabia

ARTICLE INFO

Keywords:
Ionic liquid
CO_2
Sustainable catalysis
Molecular dynamics
DFT calculations

ABSTRACT

Amino acid ionic liquids (AAILs) have gained significant attention as green solvents that are biocompatible, biodegradable, and useful in various applications, including catalysts, absorbents, and solvents. This study investigates the detailed interactions of three amino acid anions (glycine $[Gly]^-$, histidine $[His]^-$, and arginine $[Arg]^-$) with the cation 1-methoxylbutyl-3-methylimidazolium $[MOBMIM]^+$ and their role in CO_2 absorption using quantum mechanical calculations and molecular dynamics (MD) simulations. The Density Functional Theory (DFT) calculations elucidate the reaction mechanisms underlying CO_2 absorption and cycloaddition, and facilitate a comparative analysis of the impact of different amino acids on these reactions, and the synergies between them. Notably, arginine displays superior CO_2 absorption capacity in comparison to glycine and histidine. Additionally, the cycloaddition reaction with CO_2 exhibits a lower energy barrier when arginine is involved. Insights from the MD simulations highlight the higher level of electrostatic interaction between $[MOBMIM]^+[Arg]^-$ and CO_2, relative to the other studied molecules. Moreover, the Lennard Jones interaction emerges as the dominant type of interaction in these systems. The diffusion coefficient for CO_2 was highest when interacting with $[MOBMIM]^+[Gly]^-$, followed by $[MOBMIM]^+[Arg]^-$. Consequently, both MD and DFT investigations converge to suggest that $[MOBMIM]^+[Arg]^-$ followed by $[MOBMIM]^+[Gly]^-$ may serve as advantageous choices for CO_2 fixation and cycloaddition. The findings from this study underscore the considerable potential of the investigated AAILs as materials conducive to CO_2 capture and utilization, thus paving the way for the integration of CO_2 capture into valuable chemical products.

1. Introduction

One of the most crucial greenhouse gases in the atmosphere is carbon dioxide (CO_2), alongside several others. However, human activities such as intensified combustion of fossil fuels and industrial emissions have contributed to the discharge of greenhouse gases into the atmosphere. The excessive production of CO_2 by humans has played a significant role in global warming, which has resulted in unfavorable climatic changes, glacier melting, and environmental degradation. In 2021, coal and oil usage increased, resulting in the highest annual increase in CO_2 emissions ever recorded, according to the World Energy Outlook (WEO) 2021 report from the International Energy Agency (IEA) (IEA, 2022). As

* Corresponding authors.
E-mail addresses: ab_rajjak@yahoo.co.in (A.R. Shaikh), albert.poater@udg.edu (A. Poater), mohit.chawla@kaust.edu.sa (M. Chawla), luigi.cavallo@kaust.edu.sa (L. Cavallo).

https://doi.org/10.1016/j.rsurfi.2023.100175
Received 23 September 2023; Received in revised form 26 November 2023; Accepted 11 December 2023
Available online 15 December 2023

a result, total CO_2 emissions reached 36.6 Gt in 2021. The IEA has set a roadmap to achieve net-zero emissions by 2050. However, reducing emissions alone is insufficient to reach climate goals; strategies to remove existing CO_2 from the atmosphere are required. Coal power stations (run by natural gas and oil) account for 60% of all CO_2 emissions, while fossil fuels and minerals account for roughly 79% of all CO_2 emissions (IEA, 2022), according to recent analysis by the Intergovernmental Panel on Climate Change (IPCC).

The release of CO_2 is concerning because it can affect both aquatic and terrestrial life. To meet climate goals and reduce the environmental impact of anthropogenic greenhouse gases that contribute to climate change and ocean acidification, nations are interested in carbon capture (Liu et al., 2012), utilization, and storage (CCUS) technologies to remove CO_2 from the atmosphere and combustion products of hydrocarbons. Several scientific initiatives have been launched to capture CO_2 and prevent its harmful consequences. Although CO_2 capture and storage can prevent CO_2 concentration from increasing, its practical application is hampered by its high-energy consumption (Seidel et al., 2018). However, CO_2 capture and use are significant alternative strategies for reducing CO_2 emissions (Bhat and Darensbourg, 2022; Natongchai et al., 2021). There are various techniques for capturing CO_2, such as chemical and physical absorption (Hussain et al., 2021; Balchandani et al., 2022), adsorption by metallic organic frameworks (Coronado et al., 2013; Poater et al., 2018), and membrane separation (Wang et al., 2018). The scientific and technological sectors are increasingly interested in the absorption of CO_2 from various waste gases using ionic liquids (ILs), which are potential green solvents. However, materials currently used to remove CO_2 from gas streams through physical and chemical absorption and via membranes (Hussain et al., 2021; Balchandani et al., 2022; Baker and Lokhandwala, 2008) have limited efficiency and pose additional environmental concerns. These include the high cost of regenerating and replacing solvents, oxidative degradation, and the limited lifetime of carbon capture infrastructure due to the reactivity with materials. For instance, dilute aqueous alkanolamines, such as methanolamine, have a high rate of evaporation loss and are not an ideal solution. Therefore, researchers are searching for materials with more desirable properties (Yu et al., 2012).

Ionic liquids have emerged as a promising category of materials for carbon capture and storage (CCS) due to their tunable properties and potential as "green" solvents (Aghaie et al., 2018; Brennecke and Maginn, 2001; Earle and Seddon, 2000). Ionic liquids are composed of molecular ions consisting of an organic cation and either an inorganic or organic anion. Typically, they exhibit a liquid state at room temperature, possess low volatility, and exhibit high thermal stability. Due to their ability to absorb gases such as carbon dioxide and hydrogen sulfide, ionic liquids are of interest for CCS and natural gas sweetening. The low volatility of ionic liquids compared to alkanolamines also reduces solvent replacement costs and environmental impact. The ability to select the cation and anion pairs provides the opportunity to tailor the properties of ionic liquids for specific applications. As an example, glycol-bonded 1,8-diazabicyclo [5.4.0]undec-7-ene ($[DBU\text{-}PEG]^{2+}$) is a dication that can increase the solubility of CO_2 in a mixture with bis (trifluoromethylsulfonyl)imide (Tf_2N^-) up to twice that of $[EMIM]^+[Tf_2N]^-$ and $[EMIM]^+[B(CN)_4]^-$, which are known for high CO_2 solubility (Babarao and Dai, 2011). Due to their composition diversity, high thermal stability, and low vapor pressure, ionic liquids have become effective absorbents and catalysts for CO_2 chemical conversion consumption (Masoumi et al., 2023), reducing the impact of absorbent loss and degradation. To improve their properties for CCS, various strategies have been employed to develop ionic liquids with desirable properties, such as amino acid ionic liquids (AAILs) (Shaikh et al., 2016; Bao et al., 2003a; Fukumoto et al., 2005; Ohno and Fukumoto, 2007; Zhang et al., 2006), amine-functionalized ILs (Chau et al., 2013; Cao et al., 2016; Gurkan et al., 2010), phosphonium-based ILs (Zhang et al., 2006; Harper et al., 2011), and protic ionic liquids (PILs) (Greaves and Drummond, 2008; Huang et al., 2014, 2016; Zhang et al., 2020). Some ionic liquids are recyclable, which can alleviate environmental issues associated with their use.

Conventional, task-specific, and functionalized ionic liquids have been investigated for CCS applications. Brennecke et al. (Brennecke and Maginn, 2001) investigated the CO_2 solubility of common imidazolium-based ionic liquids at high pressures. Task-specific ionic liquids (TSILs) can be tailored to specific applications by adjusting the composition of ionic liquids, for example, by attaching an alkaline $–NH_2$ group to impart zwitterion character (Bao et al., 2003a). TSILs can help avoid problems associated with amine-based aqueous ionic liquids. The usage of amino acid ionic liquids (AAILs) in carbon dioxide (CO_2) capture (Onofri et al., 2020), and cycloaddition reactions has increased dramatically in recent years. AAILs were developed after their use was described by Bao et al. (AAILs) (Bao et al., 2003a). Using 1-ethyl-3--methyl imidazole ($[Emim]^+$) as the cation and 20 natural amino acids as the anions, Ohno et al. (Ohno and Fukumoto, 2007) subsequently synthesized AAILs. Ionic liquids derived from amino acids are advantageous for several reasons, including their inexpensive cost, reduced environmental effect, and biodegradability. At equilibrium, the CO_2 absorption capacity of the tetrabutylphosphonium amino acid $[P_{4444}]^+[AA]^-$ produced by Zhang et al. (2006) was 50 mol% of ILs. The amino acid anion showed more excellent CO_2 capture in ILs than the $[BF_4]^-$, Cl^-, $[NO_3]^-$, and $[PF_6]^-$ anion of the same cation. Brennecke and his colleagues also chose a series of AAILs to absorb CO_2 (Gurkan et al., 2010). They found that the amine groups in amino acid anions were better at capturing CO_2 than those in amine cation-based ILs. Imidazolium-based ILs showed greater performance for CO_2 capture and cycloaddition processes than those based on imidazolium, phosphonium, ammonium, and pyridinium, which are all extensively employed in ILs (Zhang et al., 2022; Bao et al., 2003b). To further improve the CO_2 affinity of AAILs, functional groups were introduced to the imidazolium cation in order to minimize the viscosity and heat of absorption of ILs. In addition, the energy barrier for the ring-opening phase may be lowered if the C2 proton of the imidazolium ring forms an H-bonding connection with the epoxide. However, AAILs that are very efficient at CO_2 collection and the cycloaddition reaction are extremely rare. Motivated by the aforementioned, Qu et al. (2021) synthesized a class of AAILs ($[MOBMIM]^+[AA]^-$, where [AA] can be $[Gly]^-$, $[Arg]^-$, and $[His]^-$, which feature an imidazolium cation with an ether group functionalization and an amino acid anion.

As documented by recent reviews (Greaves and Drummond, 2008; Zhang et al., 2022), the adsorption of CO_2 onto ionic liquids (ILs) has been a topic of both experimental and computational research in recent years (Hussain et al., 2011; Firaha and Kirchner, 2016). Among various techniques, Density Functional Theory (DFT) and Molecular Dynamics (MD) simulations have been successfully employed to investigate the reaction process and predict physical properties associated with CO_2 adsorption characteristics (Shaikh et al., 2015, 2020, 2022). Literature suggests that adding an ether group to the alkyl side chain of the imidazolium cation may reduce the viscosity of amino acid ionic liquids (AAILs) and enhance their CO_2 absorption efficiency. The synergistic effects of amino acid anions and ether group functionalized imidazole cations on CO_2 absorption have been found to be particularly impressive. AAILs have various benefits for CO_2 absorption, such as their structure and physio chemistry (Goel et al., 2019). Here, we perform DFT analyses and MD simulations using the MOB cation with three amino acid anions (glycine, arginine, and histidine) to investigate the effectiveness of CO_2 absorption (Qu et al., 2021). The solute electron density solvation model (SMD) is utilized to reveal mechanistic insights, specifically the transition state involved in CO_2 capture in the gas and solvent phases (both implicit and explicit solvent). Furthermore, we extensively explore the impact of cation type and the presence of two distinct aliphatic chains on the pure ILs and their structural features and dynamic properties of interest using MD simulations. Our current research aims to gain a better understanding of the reaction mechanism to design novel ionic liquids with enhanced CO_2 absorption capability.

2. Experimental

2.1. Quantum mechanical calculations

The Gaussian16 package was utilized to conduct static Density Functional Theory (DFT) calculations (Frisch et al., 2016). The M06–2X hybrid Generalized Gradient Approximation (GGA) functional, developed by Truhlar and coworkers (Zhao and Truhlar, 2006, 2008), was combined with the 6–311 + G(d) basis set for geometry optimizations (McLean and Chandler, 1980; Krishnan et al., 1980). Analytical frequency calculations were carried out to characterize the stationary points. The polarizable continuum model (PCM) was used to perform single point energy calculations, accounting for the solvent effect using ethanol as the solvent (Barone et al., 1997; Tomasi et al., 2005), following the scheme used in past studies to model the polarity of ionic liquids (Shaikh et al., 2020, 2022).

2.2. Molecular dynamics simulations

2.2.1. Force field parametrization

All molecular dynamics simulations were conducted using the Gromacs 2020 program (Abraham et al., 2015). The molecular structures of the cation [MOBMIM] and anions [Gly], [His], and [Arg] were sketched and optimized using the Gaussian program, with their structures displayed in Scheme S1. The optimized structures were utilized to carry out electrostatic potential calculations using the Merz-Kollman method at the HF/6-31G(d) level of theory, and the electrostatic potential energy surface was generated using a multiconfigurational two-stage RESP fitting. The Antechamber program of Amber Tools was employed to estimate the RESP charges for the cation and anions.

2.2.2. Molecular dynamics simulations

The AAILs initial configurations of cations and anions were generated using the Packmol program (Martinez et al., 2009), and all MD simulations were conducted using the GROMACS 2020 simulation program (Abraham et al., 2015). The Generalized Amber Force Field (GAFF) was employed for the parameterization of the ionic liquids. The choice of GAFF is based on our previous computational studies on amino acid ionic liquids (Shaikh et al., 2020, 2022). An initial minimization was performed to eliminate close contacts and achieve the minimum energy structure for further simulations. Subsequently, two steps of MD equilibration were carried out using NVT and NPT ensembles, respectively, with a simulated annealing process to increase the temperature from 0 to 600 K and then cool it down to 300 K in 50 K decrements. A 10 ns NPT simulation was performed with a pressure of 1 bar using the velocity-rescaling thermostat and the Berendsen barostat, followed by a production simulation of 100 ns using the NPT ensemble and the Parrinello−Rahman barostat (Parrinello and Rahman, 1981) with a coupling time of 2 ps. The equations of motion were integrated based on the leapfrog algorithm with a time step of 2 fs. The electrostatic interactions beyond 1.2 nm were calculated using the Particle-Mesh-Ewald (PME) method (Darden et al., 1993), and standard Periodic boundary conditions (PBCs) were applied in all directions. The Linear Constraint Solver (LINCS) algorithm (Hess et al., 1997) was utilized to constrain the hydrogen bonds.

The interaction between CO_2 and AAILs was investigated through MD simulations, utilizing the same simulation parameters as reported for neat AAILs simulation. Our MD simulations system consist of an ensemble of 80 cationic and 80 anionic molecules within a neat IL environment, as well as a corresponding system comprising 80 cations, 80 anions, and 80 carbon dioxide (CO_2) molecules, emulating the IL-CO_2 mixture. The simulations were designed to reflect a 1:1 adsorption ratio between IL:CO_2 system. The initial dimensions of the simulation cubic cell were defined as $35 \times 35 \times 35$ nm^3. Gromacs tools were employed for the analysis, and the visualization of the simulation data was performed using the VMD program (Humphrey et al., 1996).

3. Results and discussion

3.1. QM studies

Based on experimental results on ILs, the interactions between ILs and CO_2 were investigated using DFT calculations, with a focus on both CO_2 fixation and functionalization via epoxides. In the case of glycine, CO_2 fixation appeared to be a relatively simple process, as depicted in Fig. 1. However, the process involves the formation of the adduct **II** followed by the coordination of CO_2 to the N atom of the IL's anionic component (Gorantla and Mallik, 2020). Although the initial adduct **II** is thermodynamically unfavorable by 4.8 kcal/mol compared to the starting IL **I**, for entropic reasons (Falivene et al., 2018), gathering different species (Richmond et al., 2019; Gómez-Suárez et al., 2016), the subsequent kinetic barrier is relatively low, with an overall energy cost of 11.7 kcal/mol from **I** to intermediate **III**, which is less stable than **I** by up to 7.6 kcal/mol. The transition state **II-III**, shown in Fig. 2a, has characteristics of an early transition state, with a relatively long N···C distance of 2.261 Å. In **II**, the N···C distance is 2.707 Å, which is reduced to 1.646 Å in **III**. A closer analysis reveals that the C–N bond formed is fragile, unlike the already existing C–N bond (1.478 Å). This finding is supported by the Mayer Bond Orders (MBOs) analysis, which yields values of 0.656 and 0.572 for **II** and **III**, respectively, contrary to what one would expect based on bond distances. Nonetheless, both bonds are real, consistent with previous studies (Lattanzi et al., 2012; Hanifpour et al., 2020).

In order to further investigate the factors that may favor the CO_2 insertion towards intermediate **III**, a more complex pathway was explored in addition to high CO_2 pressure. The proposed pathway involves the initial binding of CO_2 to the nitrogen atom of the anionic component of the IL, with the involvement of a hydrogen atom from the NH_2 group that is transferred to one of the oxygen atom of CO_2, leading to transition state **I-IV** with an energy barrier of 38.2 kcal/mol (as shown in Fig. 2b). The presence of a water molecule in an autocatalytic form can lower the energy barrier to 28.1 kcal/mol at a temperature of 50 °C. Further addition of three water molecules can slightly reduce the energy barrier by 0.7 kcal/mol, resulting in an energy barrier of 27.4 kcal/mol (as shown in Fig. 2c). This reduction in energy barrier is attributed to the formation of a strong hydrogen bond (1.759 Å) between the two parts of the IL through the water molecules that facilitate the transfer of the hydrogen atom between the NH_2 group and the CO_2 oxygen. This interaction is remarkable since it is associated with a significant MBO of 0.091, which is rather unusual for H-bonds (Poater et al., 2018; Brotons-Rufes et al., 2023a). Thermodynamically, this pathway leads to intermediate **IV**, which is 1.6 kcal/mol more stable than **I**, with a short C–N bond of 1.359 Å and an associated MBO of only 1.233. From intermediate **IV**, a hydrogen transfer from the NH group of the 5-membered ring of the cationic component of the IL can occur kinetically through transition state **IV-V** with a barrier of 7.1 kcal/mol. Subsequently, a second CO_2 molecule can join the recently deprotonated carbon through transition state **VI-VII** (as shown in Fig. 2d), with a kinetic cost of 26.9 kcal/mol from intermediate **IV**. However, this second CO_2 fixation is less stable than the first (Mercy et al., 2016), as it leads to intermediate **VII**, which is still 3.7 kcal/mol less stable than **I**.

Alternative mechanisms were also investigated, as described in Fig. S1, to elucidate the behavior of CO_2 units with amino acids. One such mechanism involved investigating the rotation of the NH_2 amino group, however the rotation barrier was found to be only 1.4 kcal/mol, facilitating the understanding of the reactive processes, and, actually, in ionic liquids this type of rotation is rather facile. Another alternative mechanism studied the collapse of the two units with a covalent bond between the carboxylate group and the CH group between ring nitrogens of 5 members of the cationic part. Despite being barrierless, this step led to intermediate **VIII** with a thermodynamic destabilization of 21.5 kcal/mol. Subsequent coordinations of CO_2 were unfavorable, with intermediates **IX** and **X** being 40.9 and 46.5 less stable than **I**. Intermediate

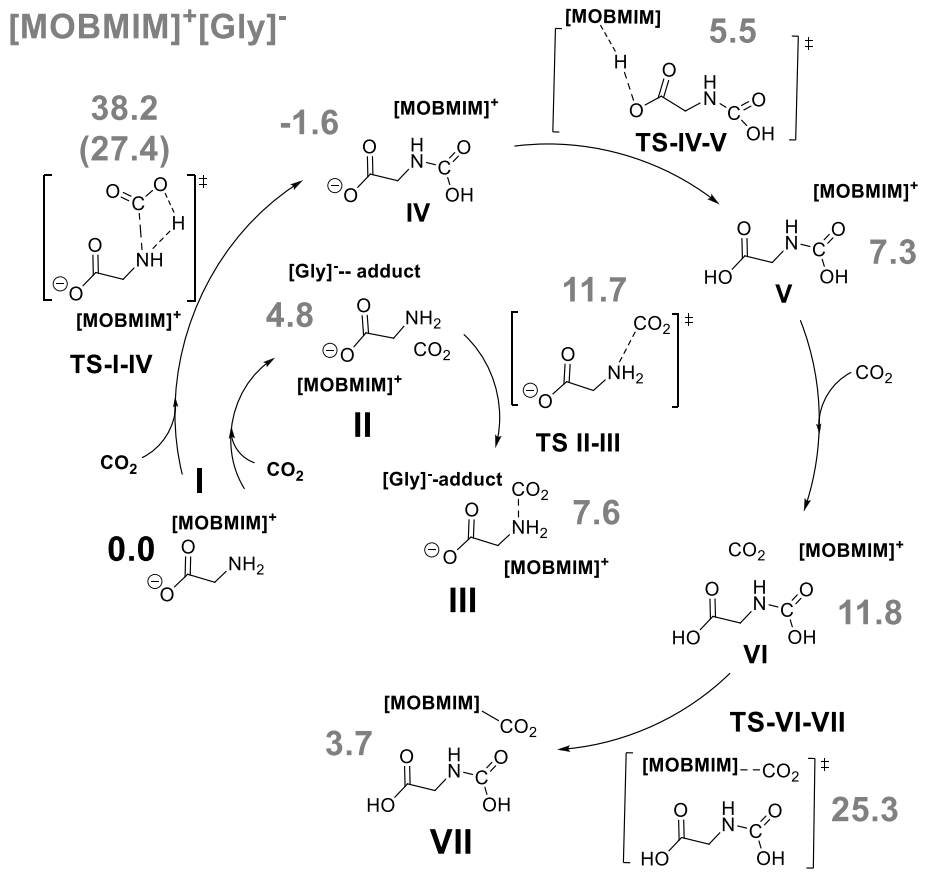

Fig. 1. The proposed mechanism for the absorption of CO_2 by the ionic liquid $[MOBMIM]^+[Gly]^-$ **I** involves the formation of the $[MOBMIM]^+[Gly]^-$-CO_2 adduct **VII** (relative Gibbs energies in kcal/mol, between parentheses the step is assisted by water molecules).

II was found to be more favorable than adduct **XI** with a CO_2 molecule simply stabilized by non-covalent interactions with the 5-membered ring, which was disfavored by 1.3 kcal/mol, and intermediate **XII** with an additional CO_2 unit near the amino group, which was disfavored by up to 10.7 kcal/mol over **I**. This interaction with the amino group was found to be completely sterile since if it becomes covalent, the destabilization is identical for intermediate **XIII**. Facilitating a proton transfer from the amino group to the more nucleophilic oxygen only stabilized by 7.7 kcal/mol, still being 3.0 kcal/mol above the resulting intermediate **XIV**. However, these intermediates must be mentioned since then they make it easier to trap in the carboxylate group the proton of the CH group between the two nitrogen atoms of the 5-membered ring of the cationic MOBMIM moiety paying only a kinetic cost of 7.6 kcal/mol, leading to the intermediate **XV**, more stable by 1.8 kcal/mol, but still 1.2 kcal/mol above **I**. At the same time, this process causes the stripped carbon to retain the CO_2 that was remaining uncoordinated. However, transferring the proton from the carboxylate group to the last CO_2 coordinated to the MOBMIM moiety is not facilitated since a relatively unstable intermediate **XVI** is reached, 22.5 kcal/mol above with respect to **I**. It must be emphasized that the transfer of the proton from the 5-membered ring of the cation to the carboxylate group in intermediate **I** is a redundant process that does not proceed since it leads to a rather unstable intermediate **XVII**, despite having only a barrier of 2.7 kcal/mol. With the inclusion of the solvent effect computationally, its resulting relative energy with respect to **I** is above the kinetic cost. The entry of CO_2 to stabilize the kinetically deprotonated carbon would require 25.6 kcal/mol, reaching intermediate **XIX**, 0.5 kcal/mol above **I**. It is then necessary to explore the interaction of CO_2 with the amine, overcoming a TS **XIX-XXI** with a kinetic cost of 15.4 kcal/mol with respect to **I**, but it would be the proton transfer step from one of the hydrogens to the last incoming CO_2 that blocks this alternative mechanism, which is still competitive since it only has one energy barrier 2.0 kcal/mol higher than that of rate determining step (rds) TS **I-IV**. However, all these alternative processes were dismissed since thermodynamic stabilization was not reached in any of them. The two nitrogen atoms of the 5-membered ring cannot accept the proton of the CH group in between, as all intermediates or transition states located following this strategy showed a huge destabilization of at least 80.1 kcal/mol. The most plausible mechanism is displayed in Fig. 1, involving a simple insertion of CO_2 up to intermediate **III**.

For the purpose of comparison with arginine and histidine, we also investigated TS **I-IV** in the presence of several water molecules. The energy barriers were found to be 21.9 and 27.0 kcal/mol, respectively. This suggests that the process should be favored with arginine, highlighting the significant electronic effect of the substituents on the methylidene of glycine. Unlike the case of simple glycine, the lowest energy barrier for TS **I-IV** is found with 3 water molecules for the other two amino acids. The energy barriers are 3.3 and 5.1 kcal/mol lower for arginine and histidine, respectively. In addition, to provide more clarity, we also studied TS **VI-VII**, with energy barriers of 24.1 and 31.0 kcal/mol, respectively. This indicates that arginine is promising in improving glycine once again by 2.8 kcal/mol. Furthermore, intermediate **IV** is found to be thermodynamically more stable by 1.5 and 5.3 kcal/mol for glycine, which could shift the equilibrium towards this amino acid. Actually, after analyzing the reaction mechanisms, it is evident that despite their computational similarities, there exists an unclear trend among the three amino acids being studied. To distinguish between the different performance of the three amino acids, non-covalent interaction (NCI) plots, developed by Contreras-García et al. (2011), are shown in Fig. 3. They unveil how important are the interactions in the intersection of the two moieties for each IL, the cationic and the anionic, i.e. the amino acid, even though the difference between them is just a sidechain

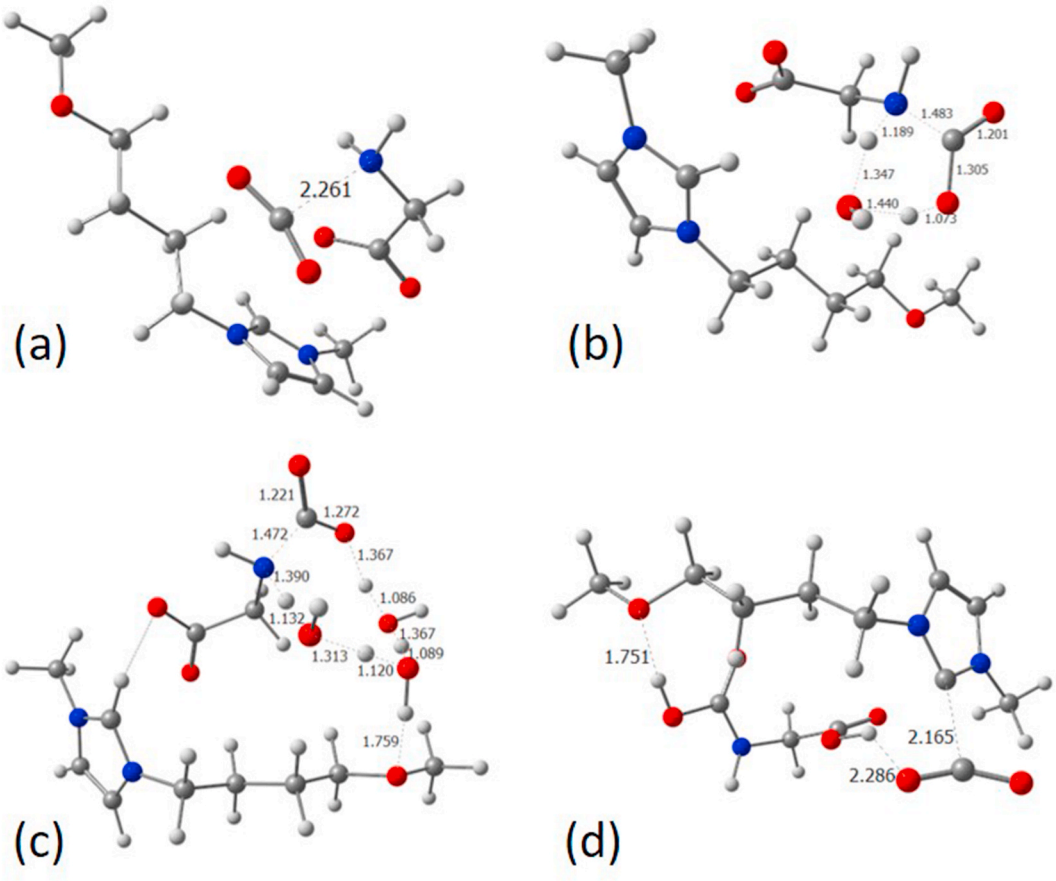

Fig. 2. Transition states (a) **II→III**, (b) **I→IV** assisted by 1 or (c) 3 water molecules and (d) transition state **VI→VII** (selected distances given in Å).

that does not participate in the intersection between both charged species (Poater et al., 2018). The absence of the sidechain for glycine in Fig. 3 leads to a stronger interaction, resulting in higher energy barriers, despite having the lowest steric hindrance. This is apparent in both 3D and 2D NCI plots. Specifically, in the latter 2D plots (Boto et al., 2020), the favorable region in dark green, close to 0.0 a. u., is more significant for the glycine system (Brotons-Rufes et al., 2023b).

To improve the comparative analysis of the three amino acids, knowing that experimentally, it is feasible to functionalize CO_2 to cyclic carbonates using epoxides (Qu et al., 2021), not at room temperature, but at a higher temperature of 110 °C, their reactivity with epoxides was also explored computationally. The epoxidation process involves three main steps, wherein the nature of the IL eliminates the need for an additional nucleophile such as tetrabutylammonium iodide (TBAI). In Fig. 4, the initial IL **I** forms a relatively unstable adduct **II'** with the epoxide, which stabilizes and progresses to intermediate **III'** after the anionic part of the IL opens the epoxide. Then, the CO_2 entry follows with TS **III'-IV'**, and the next step involves cyclization via TS **IV'-V'**. From the values in Fig. 4, it is evident that for arginine and glycine, the last two transition states are isoenergetic, with barriers of 18.6 and 21.6 kcal/mol, respectively. For histidine, the entry of CO_2 is 0.9 kcal/mol less favored, resulting in a barrier of 22.6 kcal/mol. Therefore, the opening of the epoxide is the rate-determining step, and it is favored by 2.8 and 1.9 kcal/mol for arginine, with respect to glycine and histidine, respectively (see Fig. 5). The most favorable system for epoxidation is arginine, both kinetically and thermodynamically since the cyclic carbonate already formed intermediate **V**′ is more stable than the other two types of Ils by at least 2.5 kcal/mol. The use of species **VII** as "activated CO_2" has not been considered since the energy barrier corresponding to the insertion of CO_2, defined by the TS **III'-IV'**, is not decisive and is of reduced magnitude.

To gain a deeper understanding of the interactions involved in the cyclization of epoxides with the different amino acids, Natural Bond Orbital (NBO) analyses were performed (Brotons-Rufes et al., 2023b). The different strengths of nucleophiles can be explained by observation of the orbitals involved in the attack, in this case, the p orbitals of the oxygen atom in the carboxylic moiety of each amino acid. In this case, the p orbitals' overall population is taken as a good measure of the availability of charge for the reaction. The average occupation values of the anionic oxygen atom's p orbitals (glycine = 1.694, histidine = 1.698 and arginine = 1.702, see Table S1) provide evidence of arginine's higher nucleophilic character. This trend is further confirmed by examining the charge on the oxygen, which is −0.830, −0.840 and −0.852 for glycine, histidine, and arginine, respectively (see Table S2). The Wiberg bond index matrix in the natural atomic orbitals indicates a lesser double bond character with arginine, suggesting a hybridization equilibrium more displaced to one side in Scheme 1. Furthermore, the NBO program offers a 2nd order perturbation theory analysis that helps to evaluate the convenience of donor-acceptor NBOs, which can be used to evaluate hybridization changes of structures (Brotons-Rufes et al., 2023b). In this line, the nucleophilicity of a carboxylate-based Lewis base can be related to the relative stability the molecule gains when moving electron density form the carboxyl double bond to the oxygen atomic orbitals. Specifically, the energy corresponding to the hybridization of the carboxyl bond is lower in arginine (*i.e.* relatively, electrons prefer to stay in the O lone-pairs than in the CO bond), which agrees with the populations and charges seen before (see Tables S3 and S4). Furthermore, upon examining the energies of the highest occupied molecular orbital (HOMO) in Table S5, it can be seen that arginine has the least stable HOMO (see Supplementary Information for further details).

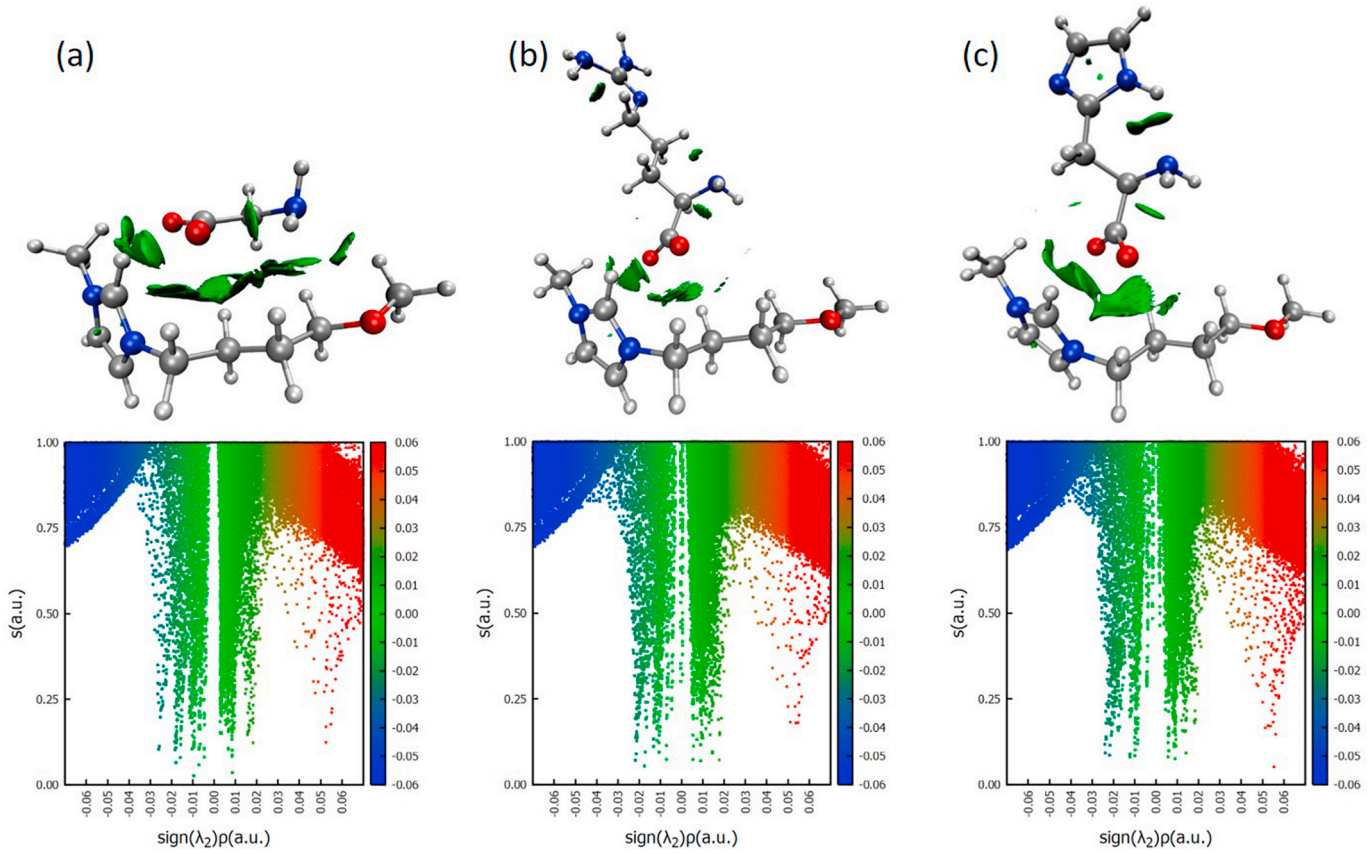

Fig. 3. 3D-NCI plots of the intermediate $[MOBMIM]^+[AA]^-$ (AA = (a) glycine, (b) arginine, (c) and histidine (above) and 2D-NCI plots of reduced density gradient (s) vs. sign (l2)r, in a. u., (below).

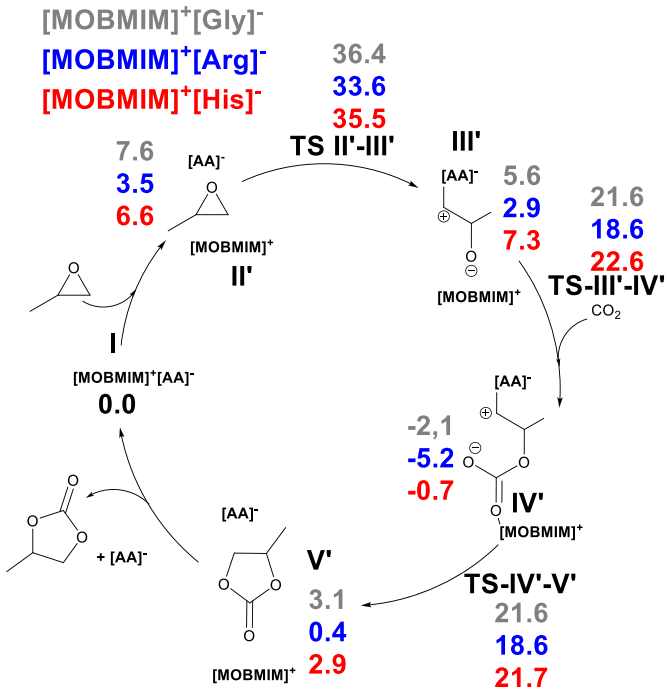

Fig. 4. Reaction pathway of the cyclization of epoxides with CO_2 catalyzed by $[MOBMIM]^+[AA]^-$ (AA = arginine, glycine and histidine) (relative Gibbs energies in kcal/mol).

3.2. MD simulations

After conducting mechanistic and energetic evaluations of AAILs with CO_2 and studying their catalytic role using DFT methods, MD simulations were employed to explore the interactions of ILs in both their neat form and in the presence of CO_2. The MD analysis aims to provide insights into the interactions between the cation, anion, and CO_2, and offers an opportunity to compare the results with those obtained from DFT calculations. By linking DFT and MD studies, a more comprehensive understanding of the behavior of ILs and their potential as catalysts for CO_2 interactions can be achieved. Initially, we analyzed the molecular density of ILs, namely $[MOBMIM]^+[Gly]^-$, $[MOBMIM]^+[His]^-$, and $[MOBMIM]^+[Arg]^-$. The densities were found to be 1.14 ± 0.1, 1.18 ± 0.1, and 1.18 ± 0.0 g/cm^3, respectively. Given the unavailability of experimental density data for the molecules under investigation, the validation of the force field was performed using MD simulations to calculate the glass transition temperature (T_g) and compare it with experimental values (Qu et al., 2021). The MD simulations included a gradual reduction in temperature by 50 K, commencing from 400 K down to 200 K. Furthermore, additional increments were performed within the temperature range of 200–225 K to precisely ascertain the T_g values. The obtained results demonstrated a satisfactory correlation between the experimental and simulated Tg values, as detailed in Table 1 and Fig. S2.

3.2.1. Self-diffusion coefficient of neat ILs and ILs in presence of CO_2

The rheological properties of Ils can be characterized by their microscopic dynamics. Atomic diffusion and viscosity are closely related properties that are associated with the dynamics of fluids (Gutowski and Maginn, 2008). While the atomic diffusion coefficient describes the diffusive transport of single particles, viscosity describes the

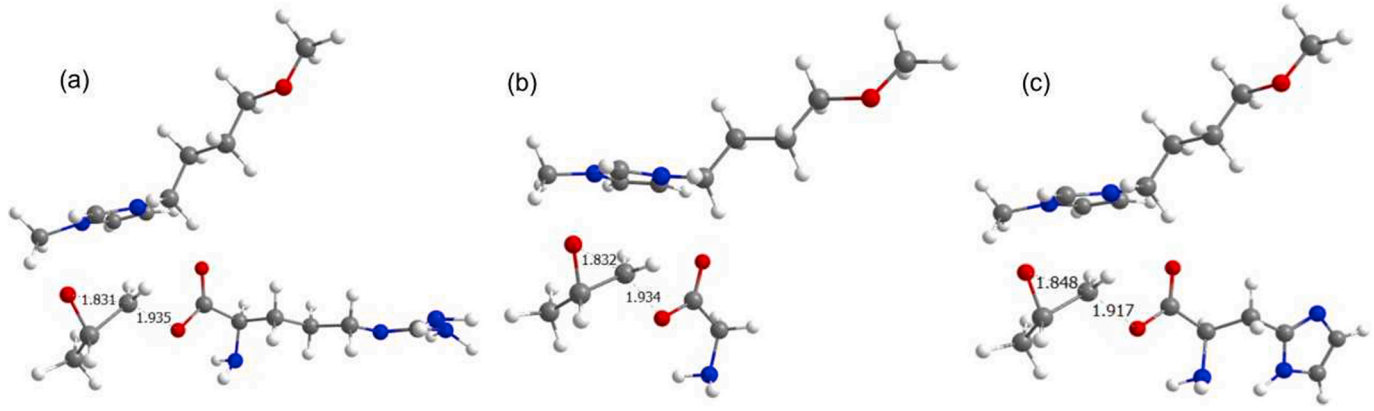

Fig. 5. Transition state **II'→III'** by (a) $[MOBMIM]^+[Arg]^-$, (b) $[MOBMIM]^+[Gly]^-$ and (c) $[MOBMIM]^+[His]^-$ (selected distances in Å).

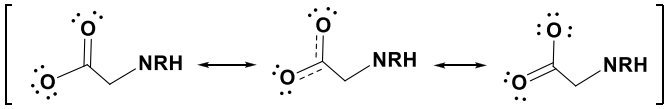

Scheme 1. Hybridization equilibrium.

Table 1
Comparison of the glass transition temperatures (T_g) of the investigated systems determined using MD simulations and experimental measurements.

Complex	T_g (K)	
	Simulations	Experimental[a]
$[MOBMIM]^+[Gly]^-$	200	205
$[MOBMIM]^+[His]^-$	220	212
$[MOBMIM]^+[Arg]^-$	215	207

[a] Experimental T_g were taken from Ref. (Qu et al., 2021).

macroscopic transport of momentum by the collective motion of the particles. It is well established that the self-diffusion coefficient (D) is inversely proportional to viscosity (Li et al., 2009). In the case of neat ILs, the self-diffusion coefficient is comparable for respective cations and anions of the investigated system. The diffusion coefficient and electrostatic interactions in ILs play a crucial role in gas absorption and separation processes, affecting CO_2 movement and absorption efficiency. These interactions influence selectivity in gas separation, impacting thermodynamics and kinetics of absorption, guiding the design of ILs for efficient and economically viable separation technologies. Understanding these factors contributes to optimized gas absorption and improved energy efficiency in separation processes. Furthermore, no significant difference was observed in the diffusion coefficient between cations and anions in neat ILs (Table 2). However, MD simulations of ILs in the presence of CO_2 showed a notable difference in the predicted diffusion coefficients. The results indicate that the diffusion coefficients for the cation and anion in IL $[MOBMIM]^+[Gly]^-$ were relatively higher compared to other ILs studied, even though there is some degree of discrepancy with past studies for the glycinate (Liu et al., 2012; Onofri et al., 2020; Firaha and Kirchner, 2016), which forced us to double check the current results. The diffusion coefficient for CO_2 was highest when interacting with $[MOBMIM]^+[Gly]^-$, followed by $[MOBMIM]^+[Arg]^-$. This suggests that the presence of $[Gly]^-$ as the anion in the IL $[MOBMIM]^+[Gly]^-$ facilitates a more favorable interaction with CO_2, leading to higher CO_2 diffusion coefficients compared to when CO_2 interacts with $[Arg]^-$ in $[MOBMIM]^+[Arg]^-$. This observation is likely attributable to the smaller size of $[Gly]^-$ in comparison to $[Arg]^-$ and $[His]^-$, which allows for enhanced interactions and increased mobility of CO_2 within the $[MOBMIM]^+[Gly]^-$ IL. Such insights are valuable for understanding the behavior of ILs in CO_2 environments and can have implications in applications such as CO_2 capture and separation processes. Further analysis of the underlying factors driving these differences could provide deeper insights into the molecular-level interactions between ILs and CO_2.

Table 2
Self-diffusion coefficients D ($\times 10^{-7}$ cm^2/s) of the respective ions in complexes of neat ionic liquids and in presence of gases.[a]

Complex/ions	[Cation]	[Anion]	$[CO_2]$
Neat Ionic Liquids			
$[MOBMIM]^+[Gly]^-$	0.03	0.02	–
$[MOBMIM]^+[His]^-$	0.01	0.01	–
$[MOBMIM]^+[Arg]^-$	0.03	0.03	–
In presence of CO_2			
$[MOBMIM]^+[Gly]^-$	0.32	0.29	6.43
$[MOBMIM]^+[His]^-$	0.01	0.01	0.28
$[MOBMIM]$ $[Arg]^-$	0.03	0.02	0.48

3.2.2. *Radial distribution functions (RDFs) for neat ils*

In order to investigate the formation of hydrogen bonds and intermolecular interactions in Ils, a radial distribution function (RDF) analysis of neat Ils was performed. The RDFs of cation-cation, cation-anion, and anion-anion pairs were plotted along with their corresponding coordination numbers, as depicted in Fig. 6. The RDF analysis was conducted using the center of geometry approach between each ion pair.

The RDF analysis of neat ILs shows that the cation-anion interaction exhibits a prominent peak at 0.49, 0.53, and 0.52 nm in $[MOBMIM]^+[Gly]^-$, $[MOBMIM]^+[His]^-$, and $[MOBMIM]^+[Arg]^-$, respectively, as depicted in Fig. 6. On the other hand, the cation-cation interaction exhibits a less distinct peak, indicating weaker interactions. Additionally, the anion-anion interaction also shows a broader peak at 0.52, 0.60, and 0.49 nm in $[MOBMIM]^+[Gly]^-$, $[MOBMIM]^+[His]^-$, and $[MOBMIM]^+[Arg]^-$, respectively.

Fig. S3 illustrates the intermolecular interactions of cation-anion, cation-cation, and anion-anion in the presence of CO_2. The interaction between cation and anion increased in $[MOBMIM]^+[His]^-$, while the other interactions did not exhibit significant changes. Overall, the strength of the cation-anion interaction appears to be higher than that of cation-cation and anion-anion interactions, as indicated by Fig. 6 and Fig. S3. Fig. S4 displays the interaction of cation-CO_2, anion-CO_2, and CO_2–CO_2. A sharp peak at 0.42 nm is observed between CO_2–CO_2, indicating a stronger interaction. These interactions are particularly stronger in $[MOBMIM]^+[His]^-$ and weaker in $[MOBMIM]^+[Gly]^-$. Moreover, RDF analysis between anion-CO_2 shows a broad peak at 0.49, 0.58, and 0.58 nm in $[MOBMIM]^+[Gly]^-$, $[MOBMIM]^+[His]^-$, and $[MOBMIM]^+[Arg]^-$, respectively. Fig. S5 presents RDF between the oxygen of $[MOBMIM]^+$ with sidechain, N-terminal N, and C-terminal O.

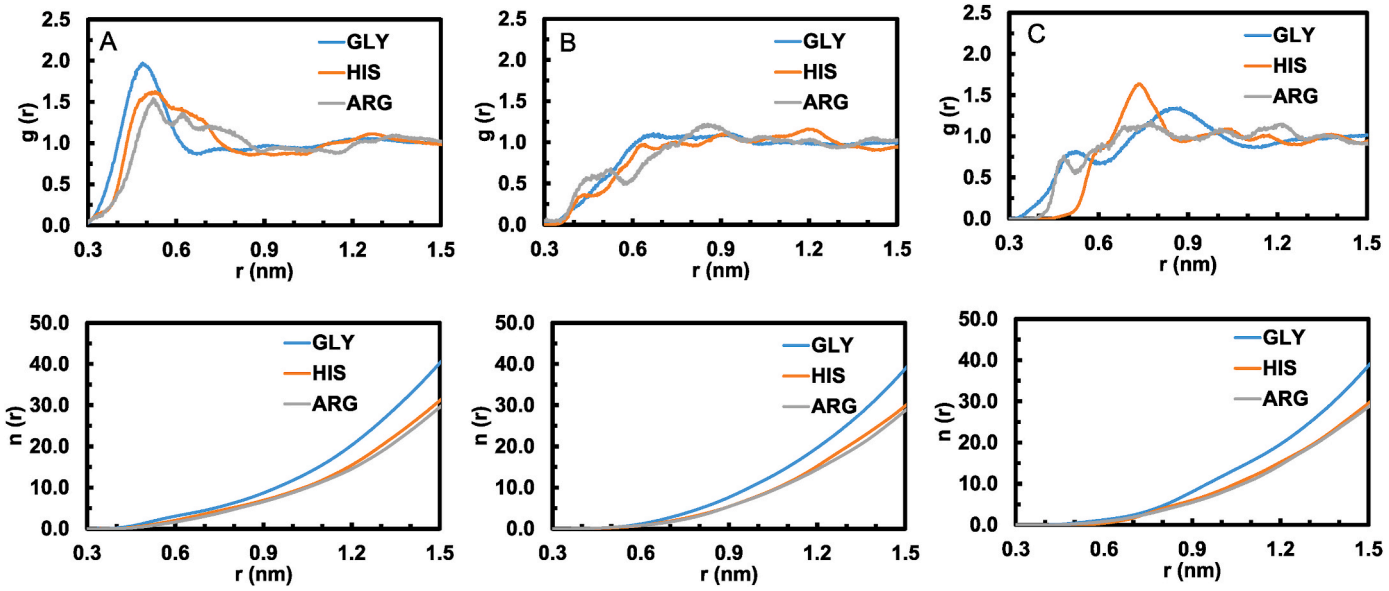

Fig. 6. Radial distribution functions (RDFs), and their corresponding coordination numbers, indicating interionic distances and ion-ion coordination in $[MOBMIM]^+[Gly]^-$, $[MOBMIM]^+[His]^-$, and $[MOBMIM]^+[Arg]^-$. RDF is shown for A) Cation-Anion, B) Cation-Cation, and C) Anion-Anion. The bottom panel shows the corresponding number integrals (n(r)) of the RDFs depicted above. Centre of mass is used to calculated RDF between different pairs.

3.2.3. *Interaction energy of cations and anions in neat ILs*

The examination of the interaction energy between the cation, anion, and CO_2 highlights a substantial interaction between these pure ILs. The total interaction energy can be partitioned into two components: the Coulombic component that accounts for electrostatic interactions and the Lennard Jones (LJ) component that primarily accounts for long-range van der Waals interactions. The average Coulombic and LJ interaction energy components between the cation and anion in neat ILs and in the presence of CO_2 is presented in Table 3.

Our results demonstrate that the Coulombic and LJ interaction energy is more favorable in $[MOBMIM]^+[Gly]^-$ compared to $[MOBMIM]^+[His]^-$ in neat ILs. Notably, the Coulombic interaction is the dominant energy contributor between cations and anions in both neat ILs and in the presence of CO_2. Specifically, our analysis reveals that the Coulombic contribution due to electrostatic interactions between cations and anions constitutes ~ >80% of the calculated interaction energy component for all the studied systems, while <20% contribution comes from the LJ interaction energy component.

Moreover, the overall interaction energy between cations and anions is reduced in the presence of CO_2, possibly due to the favorable interaction of these respective cations and anions with the CO_2 present in the system. Table 4 presents the interaction energy data for the cations and anions with CO_2. Notably, the LJ component of the interaction energy emerges as the dominant factor in the interactions between cation/anion and CO_2. Specifically, the LJ component exhibits the highest dominance in $[MOBMIM]^+[Gly]^-$, followed by $[MOBMIM]^+[His]^-$, and finally, $[MOBMIM]^+[Arg]^-$. Regarding the coulombic interactions between the anions and CO_2, the results show comparable magnitudes for $[MOBMIM]^+[Arg]^-$ and $[MOBMIM]^+[His]^-$, while the interaction energy is lower for $[MOBMIM]^+[Gly]^-$. On the other hand, when considering the coulombic interactions between the cations and CO_2, the order of dominance is $[MOBMIM]^+[Arg]^-$ > $[MOBMIM]^+[His]^-$ > $[MOBMIM]^+[Gly]^-$. These findings provide valuable insights into the relative strengths of the LJ and coulombic interactions in the studied ionic liquids when they interact with CO_2. The results contribute to a deeper understanding of the underlying forces driving these interactions, which can have implications for various applications involving CO_2 capture using ionic liquids.

Table 5 presents the results of the hydrogen bond analysis between cation-anion pairs per timeframe for both neat ILs and ILs in the presence of CO_2. Among the neat ILs, $[MOBMIM]^+[Arg]^-$ exhibits the highest number of hydrogen bonds between the cation-anion pair. However, the number of these hydrogen bonds decreases in the presence of CO_2, as the anion forms hydrogen bonds with CO_2.

Based on the comprehensive analysis, it is evident that $[MOBMIM]^+[Arg]^-$ exhibits a stronger coulombic interaction with CO_2 and

Table 3
Average interaction energy (in kcal/mol) between ions in neat ionic liquids and in presence of gases.

Complex/ions	$[MOBMIM]^+$-$[Gly]^-$/$[His]^-$/$[Arg]^-$			
	Coulombic	LJ	Coulombic	LJ
	Neat Ionic Liquids		In presence of CO_2	
$[MOBMIM]^+[Gly]^-$	−3712 ± 32	−814 ± 17	−3403 ± 38	−690 ± 17
$[MOBMIM]^+[His]^-$	−2034 ± 23	−1320 ± 19	−1900 ± 23	−1184 ± 17
$[MOBMIM]^+[Arg]^-$	−2732 ± 27	−1445 ± 23	−2489 ± 25	−1327 ± 16

Table 4
Average interaction energy (in kcal/mol) between cation and anion with CO_2.

Complex/Anion	$[MOBMIM]^+$-CO_2		$[AA]^-$-CO_2	
	Coulombic	LJ	Coulombic	LJ
$[MOBMIM]^+[Gly]^-$	−112 ± 7	−489 ± 11	−73 ± 10	−194 ± 8
$[MOBMIM]^+[His]^-$	−126 ± 7	−400 ± 9	−162 ± 11	−306 ± 8
$[MOBMIM]^+[Arg]^-$	−154 ± 8	−381 ± 9	−159 ± 12	−356 ± 10

Table 5
Hydrogen bond analysis per timeframe in neat ILs and ILs in presence of CO_2.

ILs	Hydrogen bonds		
	$[MOBMIM]^+[AA]^-$	$[MOBMIM]^+[AA]^-$	$[AA]^-$-CO_2
	Neat	In presence of CO_2	
$[MOBMIM]^+[Gly]^-$	7.4	5.9	16.0
$[MOBMIM]^+[His]^-$	7.4	5.1	20.5
$[MOBMIM]^+[Arg]^-$	14.3	10.2	30.7

forms a higher number of hydrogen bonds compared to $[MOBMIM]^+[Gly]^-$ and $[MOBMIM]^+[His]^-$. Additionally, DFT studies indicate that $[MOBMIM]^+[Arg]^-$ has a lower transition energy barrier during the cyclization of epoxide with CO_2, further emphasizing its significance. These results consistently highlight the importance of the $[MOBMIM]^+[Arg]^-$ interaction. Moreover, our findings align with experimental observations on Cholinium-amino acid ([Cho][AA]) ionic liquids, where the absorption capacities of CO_2 follow the sequence of [Cho][Arg] > [Cho][His] > [Cho][Gln] > [Cho][Glu] > [Cho][Tyr] > [Cho][Pro] (Noorani and Mehrdad, 2022). The concurrence between our results and the experimental findings reinforces the relevance of the $[MOBMIM]^+[Arg]^-$ interaction and its potential implications in various CO_2-related applications. Based on the comprehensive analysis of our DFT studies and MD simulations, we have found compelling evidence that $[MOBMIM]^+[Arg]^-$ and $[MOBMIM]^+[Gly]^-$ exhibit notably stronger interactions with CO_2. Consequently, these combinations represent the ideal candidates for CO_2 capture and cycloaddition reactions, even though with some preference for the first in agreement with past results by Mehrdad and coworkers. (Noorani and Mehrdad, 2020, 2021a, 2021b; Noorani et al., 2021, 2022).

4. Conclusions

In this investigation, we explored the interactions of three distinct AAILs using a combination of quantum mechanical and molecular dynamics simulations. The AAILs comprise an ether-functionalized imidazolium cation and an amino acid anions, and are utilized for CO_2 fixation and functionalization through epoxides, leveraging the anionic component of the ILs as a nucleophilic agent. Overall, different studies, apparently dissociated in these families of ionic liquids, are intertwined to improve the understanding of their CO_2 capture.

To confirm the interaction of AAILs with CO_2, DFT calculations were employed to investigate the details of the interaction of the ILs with CO_2, including different types of interaction, and kinetics. The results demonstrated that the interaction is more favorable with one unit of CO_2 than with two units of CO_2. Various computational predictions, including structural analyses such as MBOs and NCI plots, were used to understand the greater ease of the system with arginine. Additionally, the cyclization with epoxides was investigated, and the results indicated that the ionic liquid based on arginine was the most favorable, owing to a lower cost in the opening of the epoxide in the rate-determining step.

MD simulations were utilized to determine the radial distribution function, diffusion coefficient, interaction energy, and hydrogen bond analysis of the ILs with different amino acids as anions. These analyses provided further insight into the nature of interaction between the ILs and the amino acid anions. The interaction between the cation and anion is predominantly favored by electrostatic interaction, whereas the interaction between the ions and CO_2 is primarily favored by Lennard Jones interaction. Consistent with experimental results, both DFT and MD simulations indicated that $[MOBMIM]^+[Gly]^-$ and $[MOBMIM]^+[Arg]^-$ exhibits superior activity for CO_2 fixation and epoxide formation. As a result, the ILs studied in this study hold great potential as materials for the integration of CO_2 capture and utilization.

CRediT authorship contribution statement

Abdul Rajjak Shaikh: Conceptualization, Investigation, Methodology, Writing - original draft, Writing - review & editing. **Anna Vidal-López:** Formal analysis, Methodology, Software. **Artur Brotons-Rufes:** Data curation, Methodology, Software. **Jason J. Pajski:** Data curation, Formal analysis, Software. **Sadain Zafar:** Data curation, Formal analysis, Software. **Raisul Awal Mahmood:** Data curation, Formal analysis, Software. **Muhammad Usman Khan:** Methodology. **Albert Poater:** Funding acquisition, Methodology, Supervision, Writing - review & editing. **Mohit Chawla:** Formal analysis, Investigation, Writing - original draft. **Luigi Cavallo:** Funding acquisition, Project administration, Supervision.

Declaration of competing interest

The authors declare the following financial interests/personal relationships which may be considered as potential competing interests: Dr. Abdul Rajjak Shaikh was employed by the company STEMskills Research and Education Lab Private Limited, India. The remaining authors declare that the research was conducted in the absence of any commercial or financial relationships that could be construed as a potential conflict of interest.

Data availability

Data will be made available on request.

Acknowledgments

Authors would like to thank the King Abdullah University of Science and Technology (KAUST) Supercomputing Laboratory (KSL) for providing the necessary computational resources. We thank the Spanish Ministerio de Ciencia e Innovación for project PID 2021-127423NB-I00 and the Generalitat de Catalunya for project 2021SGR623. A.P. is a Serra Húnter Fellow and ICREA Academia Prize 2019. J.P.P, S.Z., R.M, M.K thank STEMskills Research and Education Lab Private Limited, India for providing supervision within the workshop 'MD simulations of Ionic Liquids'. We thank the reviewers for helpful comments.

Appendix A. Supplementary data

Supplementary data to this article can be found online at https://doi.org/10.1016/j.rsurfi.2023.100175.

References

Abraham, M.J., Murtola, T., Schulz, R., Páll, S., Smith, J.C., Hess, B., Lindahl, E., 2015. GROMACS: high performance molecular simulations through multi-level parallelism from laptops to supercomputers. SoftwareX 1–2, 19–25. https://doi.org/10.1016/j.softx.2015.06.001.

Aghaie, M., Rezaei, N., Zendehboudi, S., 2018. A systematic review on CO_2 capture with ionic liquids: current status and future prospects. Renewable Sustainable Energy Rev. 96, 502–525. https://doi.org/10.1016/j.rser.2018.07.004.

Babarao, R., Dai, S., 2011. Understanding the high solubility of CO_2 in an ionic liquid with the tetracyanoborate anion. J. Phys. Chem. B 115, 9789–9794. https://doi.org/10.1021/jp205399r.

Baker, R.W., Lokhandwala, K., 2008. Natural gas processing with membranes: an overview. Ind. Eng. Chem. Res. 47, 2109–2121. https://doi.org/10.1021/ie071083w.

Balchandani, S.C., Dey, A., Mandal, B., Kumar, A., Dharaskar, S., 2022. Elucidating the important thermophysical characterization properties of amine activated hybrid novel solvents for designing post-combustion CO_2 capture unit. J. Mol. Liq. 355, 118919 https://doi.org/10.1016/j.molliq.2022.118919.

Bao, W., Wang, Z., Li, Y., 2003a. Synthesis of chiral ionic liquids from natural amino acids. J. Org. Chem. 68, 591–593. https://doi.org/10.1021/jo020503i.

Bao, W.L., Wang, Z.M., Li, Y.X., 2003b. Synthesis of chiral ionic liquids from natural amino acids. J. Org. Chem. 68, 591–593. https://doi.org/10.1021/jo020503i.

Barone, V., Cossi, M., Tomasi, J., 1997. A new definition of cavities for the computation of solvation free energies by the polarizable continuum model. J. Chem. Phys. 107, 3210. https://doi.org/10.1063/1.474671.

Bhat, G.A., Darensbourg, D.J., 2022. Progress in the catalytic reactions of CO_2 and epoxides to selectively provide cyclic or polymeric carbonates. Green Chem. 24, 5007–5034. https://doi.org/10.1039/d2gc01422j.

Boto, R.A., Peccati, F., Laplaza, R., Quan, C., Carbone, A., Piquemal, J.-P., Maday, Y., Contreras-García, J., 2020. NCIPLOT4: fast, robust, and quantitative analysis of noncovalent interactions. J. Chem. Theor. Comput. 16, 4150–4158. https://doi.org/10.1021/acs.jctc.0c00063.

Brennecke, J.F., Maginn, E.J., 2001. Ionic liquids: innovative fluids for chemical processing. AIChE J. 47, 2384–2389. https://doi.org/10.1002/aic.690471102.

Brotons-Rufes, A., Bahri-Laleh, N., Poater, A., 2023a. H-Bonding leading to latent initiators for olefin metathesis polymerization. Faraday Discuss 244, 252–268. https://doi.org/10.1039/D2FD00163B.

Brotons-Rufes, A., Bahri-Laleh, N., Poater, A., 2023b. H-Bonding leading to latent initiators for olefin metathesis polymerization. Faraday Discuss. https://doi.org/10.1039/D2FD00163B.

Cao, B., Du, J., Liu, S., Zhu, X., Sun, X., Sun, H., Fu, H., 2016. Carbon dioxide capture by amino-functionalized ionic liquids: DFT based theoretical analysis substantiated by FT-IR investigation. RSC Adv. 6, 10462–10470. https://doi.org/10.1039/C5RA23959A.

Chau, J., Obuskovic, G., Jie, X.M., Mulukutla, T., Sirkar, K.K., 2013. Solubilities of CO_2 and helium in an ionic liquid containing poly(amidoamine) dendrimer gen 0. Ind. Eng. Chem. Res. 52, 10484–10494. https://doi.org/10.1021/ie303426q.

Contreras-García, J., Johnson, E.R., Keinan, S., Chaudret, R., Piquemal, J.P., Beratan, D. N., Yang, W., 2011. NCIPLOT: a program for plotting noncovalent interaction regions. J. Chem. Theor. Comput. 7, 625–632. https://doi.org/10.1021/ct100641a.

Coronado, E., Giménez-Marqués, M., Mínguez Espallargas, G., Rey, F., Vitórica-Yrezábal, I.J., 2013. Spin-crossover modification through selective CO_2 sorption. J. Am. Chem. Soc. 135, 15986–15989. https://doi.org/10.1021/ja407135k.

Darden, T., York, D., Pedersen, L., 1993. Particle mesh ewald - an N.log(N) method for ewald sums in large systems. J. Chem. Phys. 98, 10089–10092. https://doi.org/10.1063/1.464397.

Earle, M.J., Seddon, K.R., 2000. Ionic liquids. Green solvents for the future. Pure Appl. Chem. 72, 1391–1398. https://doi.org/10.1351/pac200072071391.

Falivene, L., Barone, V., Talarico, G., 2018. Unraveling the role of entropy in tuning unimolecular. Mol. Catal. 452, 138–144. https://doi.org/10.1016/j.mcat.2018.04.012.

Firaha, D.S., Kirchner, B., 2016. Tuning the carbon dioxide absorption in amino acid ionic liquids. ChemSusChem 9, 1591–1599. https://doi.org/10.1002/cssc.201600126.

Frisch, M.J., Trucks, G.W., Schlegel, H.B., Scuseria, G.E., Robb, M.A., Cheeseman, J.R., Scalmani, G., Barone, V., Petersson, G.A., Nakatsuji, H., Li, X., Caricato, M., Marenich, A.V., Bloino, J., Janesko, B.G., Gomperts, R., Mennucci, B., Hratchian, H. P., Ortiz, J.V., Izmaylov, A.F., Sonnenberg, J.L., Williams-Young, D., Ding, F., Lipparini, F., Egidi, F., Goings, J., Peng, B., Petrone, A., Henderson, T., Ranasinghe, D., Zakrzewski, V.G., Gao, J., Rega, N., Zheng, G., Liang, W., Hada, M., Ehara, M., Toyota, K., Fukuda, R., Hasegawa, J., Ishida, M., Nakajima, T., Honda, Y., Kitao, O., Nakai, H., Vreven, T., Throssell, K., Montgomery Jr., J.A., Peralta, J.E., Ogliaro, F., Bearpark, M.J., Heyd, J.J., Brothers, E.N., Kudin, K.N., Staroverov, V.N., Keith, T.A., Kobayashi, R., Normand, J., Raghavachari, K., Rendell, A.P., Burant, J. C., Iyengar, S.S., Tomasi, J., Cossi, M., Millam, J.M., Klene, M., Adamo, C., Cammi, R., Ochterski, J.W., Martin, R.L., Morokuma, K., Farkas, O., Foresman, J.B., Fox, D.J., 2016. Gaussian16. Revision C.01, Wallingford, CT.

Fukumoto, K., Yoshizawa, M., Ohno, H., 2005. Room temperature ionic liquids from 20 natural amino acids. J. Am. Chem. Soc. 127, 2398–2399. https://doi.org/10.1021/ja043451i.

Goel, H., Windom, Z.W., Jackson, A.A., Rai, N., 2019. CO_2 sorption in triethyl(butyl) phosphonium 2-cyanopyrrolide ionic liquid via first principles simulations. J. Mol. Liq. 292, 111323 https://doi.org/10.1016/j.molliq.2019.111323.

Gómez-Suárez, A., Oonishi, Y., Martin, A.R., Vummaleti, S.V.C., Nelson, D.J., Cordes, D. B., Slawin, A.M.Z., Cavallo, L., Nolan, S.P., Poater, A., 2016. On the mechanism of the digold(I)-Hydroxide-Catalysed hydrophenoxylation of alkynes. Chem. Eur J. 22, 1125–1132. https://doi.org/10.1002/chem.201503097.

Gorantla, K.R., Mallik, B.S., 2020. Reaction mechanism and free energy barriers for the chemisorption of CO_2 by ionic entities. J. Phys. Chem. A 124, 4836–4848. https://doi.org/10.1021/acs.jpca.9b06817.

Greaves, T.L., Drummond, C.J., 2008. Protic ionic liquids: properties and applications. Chem. Rev. 108, 206–237. https://doi.org/10.1021/cr068040u.

Gurkan, B.E., de la Fuente, J.C., Mindrup, E.M., Ficke, L.E., Goodrich, B.F., Price, E.A., Schneider, W.F., Brennecke, J.F., 2010. Equimolar CO_2 absorption by anion-functionalized ionic liquids. J. Am. Chem. Soc. 132, 2116–2117. https://doi.org/10.1021/ja909305t.

Gutowski, K.E., Maginn, E.J., 2008. Amine-functionalized task-specific ionic liquids: a mechanistic explanation for the dramatic increase in viscosity upon complexation with CO_2 from molecular simulation. J. Am. Chem. Soc. 130, 14690–14704. https://doi.org/10.1021/ja804654b.

Hanifpour, A., Bahri-Laleh, N., Nekoomanesh-Haghighi, M., Poater, A., 2020. Coordinative chain transfer polymerization of 1-decene in the presence of A Ti-based diamine bis(phenolate) catalyst: a green approach to produce low viscosity PAOs. Green Chem. 22, 4617–4626. https://doi.org/10.1039/D0GC00439A.

Harper, N.D., Nizio, K.D., Hendsbee, A.D., Masuda, J.D., Robertson, K.N., Murphy, L.J., Johnson, M.B., Pye, C.C., Clyburne, J.A.C., 2011. Survey of carbon dioxide capture in phosphonium-based ionic liquids and end-capped polyethylene glycol using DETA (DETA = diethylenetriamine) as a model absorbent. Ind. Eng. Chem. Res. 50, 2822–2830. https://doi.org/10.1021/ie101734h.

Hess, B., Bekker, H., Berendsen, H.J.C., Fraaije, J.G.E.M., 1997. LINCS: a linear constraint solver for molecular simulations. J. Comput. Chem. 18, 1463–1472. https://doi.org/10.1002/(SICI)1096-987X(199709)18:12%3C1463::AID-JCC4%3E3.0.CO;2-H.

Huang, K., Zhang, X., Xu, Y., Wu, Y., Hu, X., Xu, Y., 2014. Protic ionic liquids for the selective absorption of H_2S from CO_2: thermodynamic analysis. AIChE J. 4232–4240. https://doi.org/10.1002/aic.14634.

Huang, K., Zhang, X., Hu, X., Wu, Y., 2016. Hydrophobic protic ionic liquids tethered with tertiary amine group for highly efficient and selective absorption of H_2S from CO_2. AIChE J. 62, 4480–4490. https://doi.org/10.1002/aic.15363.

Humphrey, W., Dalke, A., Schulten, K., 1996. VMD: visual molecular dynamics. J. Mol. Graph. 14, 33–38. https://doi.org/10.1016/0263-7855(96)00018-5.

Hussain, M.A., Soujanya, Y., Sastry, G.N., 2011. Evaluating the efficacy of amino acids as CO_2 capturing agents: a first principles investigation. Environ. Sci. Technol. 45, 8582–8588. https://doi.org/10.1021/es2019725.

Hussain, S., Dong, H., Zeng, S., Ahmad, M.U., Shehzad, F.K., Wu, H., Zhang, Y., 2021. Investigation uncovered the impact of anions on CO_2 absorption by low viscous ether functionalized pyridinium ionic liquids. J. Mol. Liq. 336, 116362 https://doi.org/10.1016/j.molliq.2021.116362.

IEA, 2022. World Energy Outlook 2022. IEA, Paris. https://www.iea.org/reports/world-energy-outlook-2022. License: CC BY 4.0 (report); CC BY NC SA 4.0 (Annex A).

Krishnan, R., Binkley, J.S., Seeger, R., Pople, J.A., 1980. Self-consistent molecular orbital methods. XX. A basis set for correlated wave functions. J. Chem. Phys. 72, 650–654. https://doi.org/10.1063/1.438955.

Lattanzi, A., De Fusco, C., Russo, A., Poater, A., Cavallo, L., 2012. Hexafluorobenzene: a powerful solvent for a noncovalent stereoselective organocatalytic Michael addition reaction. Chem. Commun. 48, 1650–1652. https://doi.org/10.1039/c2cc17488j.

Li, C., Wang, Y., Pielak, G.J., 2009. Translational and rotational diffusion of a small globular protein under crowded conditions. J. Phys. Chem. B 113, 13390–13392. https://doi.org/10.1021/jp907744m.

Liu, A.-H., Ma, R., Song, C., Yang, Z.-Z., Yu, A., Cai, Y., He, L.-N., Zhao, Y.-N., Yu, B., Song, Q.-W., 2012. Equimolar CO_2 capture by N-substituted amino acid salts and subsequent conversion. Angew. Chem. Int. Ed. 51, 11306–11310. https://doi.org/10.1002/anie.201205362.

Martinez, L., Andrade, R., Birgin, E.G., Martinez, J.M., 2009. PACKMOL: a package for building initial configurations for molecular dynamics simulations. J. Comput. Chem. 30, 2157–2164. https://doi.org/10.1002/jcc.21224.

Masoumi, Z., Tayebi, M., Tayebi, M., Masoumi Lari, S.A., Swwandi, N., Seo, B., Lim, C.-S., Kim, H.-G., Kyung, D., 2023. Electrocatalytic reactions for converting CO_2 to value-added products: recent progress and emerging trends. Int. J. Mol. Sci. 24, 9952. https://doi.org/10.3390/ijms24129952.

McLean, A.D., Chandler, G.S., 1980. Contracted Gaussian basis sets for molecular calculations. I. Second row atoms, Z=11–18. J. Chem. Phys. 72, 5639–5648. https://doi.org/10.1063/1.438980.

Mercy, M., de Leeuw, N.H., Bell, R.G., 2016. Mechanisms of CO_2 capture in ionic liquids: a computational perspective. Faraday Discuss 192, 479–492. https://doi.org/10.1039/C6FD00081A.

Natongchai, W., Luque-Urrutia, J.A., Phungpanya, C., Solà, M., D'Elia, V., Poater, A., Zipse, H., 2021. Cycloaddition of CO_2 to epoxides by highly nucleophilic 4-amino-pyridines: establishing a relationship between carbon basicity and catalytic performance by experimental and DFT investigations. Org. Chem. Front. 8, 613–627. https://doi.org/10.1039/d0qo01327g.

Noorani, N., Mehrdad, A., 2020. CO_2 solubility in some amino acid-based ionic liquids: measurement, correlation and DFT studies. Fluid Phase Equil. 517, 112591 https://doi.org/10.1016/j.fluid.2020.112591.

Noorani, N., Mehrdad, A., 2021a. Experimental and theoretical study of CO_2 sorption in biocompatible and biodegradable cholinium-based ionic liquids. Sep. Purif. Technol. 254, 117609 https://doi.org/10.1016/j.seppur.2020.117609.

Noorani, N., Mehrdad, A., 2021b. Cholinium-amino acid ionic liquids as biocompatible agents for carbon dioxide absorption. J. Mol. Liq. 357, 119078 https://doi.org/10.1016/j.molliq.2022.119078.

Noorani, N., Mehrdad, A., 2022. Cholinium-amino acid ionic liquids as biocompatible agents for carbon dioxide absorption. J. Mol. Liq. 357, 119078 https://doi.org/10.1016/j.molliq.2022.119078.

Noorani, N., Mehrdad, A., Ahadzadeh, I., 2021. CO_2 absorption in amino acid-based ionic liquids: experimental and theoretical studies. Fluid Phase Equil. 547, 113185 https://doi.org/10.1016/j.fluid.2021.113185.

Noorani, N., Mehrdad, A., Zarei diznab, R., 2022. Thermodynamic study on carbon dioxide absorption in vinyl imidazolium–amino acid ionic liquids. Fluid Phase Equil. 557, 113433 https://doi.org/10.1016/j.fluid.2022.113433.

Ohno, H., Fukumoto, K., 2007. Amino acid ionic liquids. Acc. Chem. Res. 40, 1122–1129. https://doi.org/10.1021/ar700053z.

Onofri, S., Adenusi, H., Le Donne, A., Bodo, E., 2020. CO_2 capture in ionic liquids based on amino acid anions with protic side chains: a computational assessment of kinetically efficient reaction mechanisms. ChemistryOpen 9, 1153–1160. https://doi.org/10.1002/open.202000275.

Parrinello, M., Rahman, A., 1981. Polymorphic transitions in single-crystals - a new molecular-dynamics method. J. Appl. Phys. 52, 7182–7190. https://doi.org/10.1063/1.328693.

Poater, J., Gimferrer, M., Poater, A., 2018. Covalent and ionic capacity of MOFs to sorb small gas molecules. Inorg. Chem. 57, 6981–6990. https://doi.org/10.1021/acs.inorgchem.8b00670.

Qu, Y., Lan, J., Chen, Y., Sun, J., 2021. Amino acid ionic liquids as efficient catalysts for CO_2 capture and chemical conversion with epoxides under metal/halogen/cocatalyst/solvent free conditions. Sustain. Energy Fuels 5, 2494–2503. https://doi.org/10.1039/d1se00060h.

Richmond, C.J., Escayola, S., Poater, A., 2019. Axial ligand effects of Ru-bda complexes in the O–O bond formation via the I2M bimolecular mechanism in water oxidation catalysis. Eur. J. Inorg. Chem. 2019, 2101–2108. https://doi.org/10.1002/ejic.201801450.

Seidel, C., Jörke, A., Vollbrecht, B., Seidel-Morgenstern, A., Kienle, A., 2018. Kinetic modeling of methanol synthesis from renewable resources. Chem. Eng. Sci. 175, 130–138. https://doi.org/10.1016/j.ces.2017.09.043.

Shaikh, A.R., Kamio, E., Takaba, H., Matsuyama, H., 2015. Effects of water concentration on the free volume of amino acid ionic liquids investigated by molecular dynamics simulations. J. Phys. Chem. B 119, 263–273. https://doi.org/10.1021/jp5095239.

Shaikh, A.R., Karkhanechi, H., Kamio, E., Yoshioka, T., Matsuyama, H., 2016. Quantum mechanical and molecular dynamics simulations of dual-amino-acid ionic liquids for CO_2 capture. J. Phys. Chem. C 120, 27734–27745. https://doi.org/10.1021/acs.jpcc.6b07305.

Shaikh, A.R., Ashraf, M., AlMayef, T., Chawla, M., Poater, A., Cavallo, L., 2020. Amino acid ionic liquids as potential candidates for CO_2 capture: combined density

functional theory and molecular dynamics simulations. Chem. Phys. Lett. 745, 137239 https://doi.org/10.1016/j.cplett.2020.137239.

Shaikh, A.R., Posada-Pérez, S., Brotons-Rufes, A., Pajski, J.J., Vajiha, Kumar, G., Mateen, A., Poater, A., Solà, M., Chawla, M., Cavallo, L., 2022. Selective absorption of H_2S and CO_2 by azole based protic ionic liquids: a combined Density Functional Theory and Molecular Dynamics study. J. Mol. Liq. 367, 120558 https://doi.org/10.1016/j.molliq.2022.120558.

Tomasi, J., Mennucci, B., Cammi, R., 2005. Quantum mechanical continuum solvation models. Chem. Rev. 105, 2999–3094. https://doi.org/10.1021/cr9904009.

Wang, L.-Y., Xu, Y.-L., Li, Z.-D., Wei, Y.-N., Wei, J.-P., 2018. CO_2/CH_4 and H_2S/CO_2 selectivity by ionic liquids in natural gas sweetening. Energy Fuel. 32, 1023. https://doi.org/10.1021/acs.energyfuels.7b02852.

Yu, C.-H., Huang, C.-H., Tan, C.-S., 2012. A review of CO_2 capture by absorption and adsorption. Aerosol Air Qual. Res. 12, 745–769. https://doi.org/10.4209/aaqr.2012.05.0132.

Zhang, J., Zhang, S., Dong, K., Zhang, Y., Shen, Y., Lv, X., 2006. Supported absorption of CO_2 by tetrabutylphosphonium amino acid ionic liquids. Chem. Eur J. 12, 4021–4026. https://doi.org/10.1002/chem.200501015.

Zhang, X., Xiong, W., Peng, L., Wu, Y., Hu, X., 2020. Highly selective absorption separation of H_2S and CO_2 from CH_4 by novel azole-based protic ionic liquids. AIChE J. 66, e16936 https://doi.org/10.1002/aic.16936.

Zhang, R., Ke, Q., Zhang, Z., Zhou, B., Cui, G., Lu, H., 2022. Tuning functionalized ionic liquids for CO_2 capture. Int. J. Mol. Sci. 23, 11401 https://doi.org/10.3390/ijms231911401.

Zhao, Y., Truhlar, D.G., 2006. A new local density functional for main-group thermochemistry, transition metal bonding, thermochemical kinetics, and noncovalent interactions. J. Chem. Phys. 125, 194101 https://doi.org/10.1063/1.2370993.

Zhao, Y., Truhlar, D.G., 2008. The M06 suite of density functionals for main group thermochemistry, thermochemical kinetics, noncovalent interactions, excited states, and transition elements: two new functionals and systematic testing of four M06-class functionals and 12 other functionals. Theor. Chem. Acc. 120, 215–241. https://doi.org/10.1007/s00214-007-0310-x.